

μ SR study of unconventional pairing symmetry in the quasi-1D $\text{Na}_2\text{Cr}_3\text{As}_3$ superconductor

A Bhattacharyya^{1*}, D T Adroja^{2,3}, Y Feng^{4,5}, Debarchan Das⁶,
P K Biswas², Tanmoy Das^{7†}, J. Zhao⁴

¹ Department of Physics, Ramakrishna Mission Vivekananda Educational and Research Institute, Belur Math, Howrah 711202, West Bengal, India

² ISIS Facility, Rutherford Appleton Laboratory, Chilton, Didcot Oxon, OX11 0QX, United Kingdom

³ Highly Correlated Matter Research Group, Physics Department, University of Johannesburg, PO Box 524, Auckland Park 2006, South Africa

⁴ State Key Laboratory of Surface Physics and Department of Physics, Fudan University, Shanghai 200433, China

⁵ CSNS, 1 Zhongziyuan Road, Dalang, Dongguan, China

⁶ Laboratory for Muon Spin Spectroscopy, Paul Scherrer Institute, CH-5232 Villigen PSI, Switzerland

⁷ Department of Physics, Indian Institute of Science, Bangalore 560012, India

E-mail: *amitava.bhattacharyya@rkmvu.ac.in,

† tnmydas@gmail.com

Abstract.

We report the finding of a novel pairing state in a newly discovered superconductor $\text{Na}_2\text{Cr}_3\text{As}_3$. This material has a noncentrosymmetric quasi-one-dimensional crystal structure and is superconducting at $T_C \sim 8.0$ K. We find that the magnetic penetration depth data suggests the presence of a nodal line p_z -wave pairing state with zero magnetic moment using transverse-field muon-spin rotation (TF- μ SR) measurements. The nodal gap observed in $\text{Na}_2\text{Cr}_3\text{As}_3$ compound is consistent with that observed in isostructural $(\text{K,Cs})_2\text{Cr}_3\text{As}_3$ compounds using TF- μ SR measurements. The observed pairing state is consistent with a three-band model spin-fluctuation calculation, which reveals the $S_z = 0$ spin-triplet pairing state with the $\sin k_z$ pairing symmetry. The long-sought search for chiral superconductivity with topological applications could be aided by such a novel triplet $S_z = 0$ p -wave pairing state.

Keywords. Triplet superconductor; Superconducting gap structure; Muon spin spectroscopy

PACS numbers: 74.78.-w, 74.20.Rp, 74.25.Jb, 76.75.+i

1. Introduction

The quest for spin-triplet superconductors in which Cooper pairs have finite angular momentum and equal spin, has been one of the significant research efforts notably due to its natural link to topologically related science and for possible unconventional superconductivity [1]. To date, the most promising systems for spin-triplet superconductivity are Uranium based heavy-fermion compounds UTe_2 [2], UGe_2 [3], UPt_3 [4], as well as Sr_2RuO_4 [1]. From the theoretical viewpoint [1], spin-triplet Cooper pairs are thought to originate directly from ferromagnetic (FM) fluctuations. Superconductivity in the vicinity of an antiferromagnetic (AFM) instability has been extensively explored in the last three decades or so [5] as in the case of high-temperature cuprates [6], iron pnictides [7] and heavy fermion systems [8]. Superconducting materials with a background of FM spin fluctuations are still rare, as observed A-phase of super-fluid ^3He [9].

In inorganic quasi one dimensional (Q1D) $3d$ -electron system, $\text{A}_2\text{Cr}_3\text{As}_3$ ($\text{A} = \text{Na}, \text{K}, \text{Rb}$, and Cs), which crystallize in the noncentrosymmetric hexagonal structure with space group $P\bar{6}m2$ (No. 187) [10], it has been confirmed that the upper critical field H_{c2} perpendicular to Cr-chain is significantly larger than the Pauli limit, which strongly supports spin-triplet pairing [11]. Moreover a nodal line gap symmetry was unveiled by magnetic penetration depth measurement on $(\text{K,Cs})_2\text{Cr}_3\text{As}_3$ [12–14] and Volovik-like field dependence of the zero-temperature Sommerfeld coefficients in the SC mixed state of $\text{A}_2\text{Cr}_3\text{As}_3$ [15]. The spin-lattice relaxation rate ($1/T_1$) of $\text{A}_2\text{Cr}_3\text{As}_3$ decreases rapidly below T_C with no Hebel-Slichter peak and ubiquitously follows a T^5 variation below a characteristic temperature $\sim 0.6 T_C$, which indicates the existence of nodes in the superconducting gap function and ferromagnetic spin fluctuations within the sublattice of Cr atoms [16]. Neutron scattering measurements suggest subtle interplays of structure, electron-phonon, and magnetic interactions in $\text{K}_2\text{Cr}_3\text{As}_3$ [17]. A recent, ^{75}As nuclear quadrupole resonance study [16] suggests that the temperature dependence of the $1/T_1$, by changing A in the order of $\text{A} = \text{Na}, \text{Na}_{0.75}\text{K}_{0.25}, \text{K}$, and Rb , the system can be tuned to approach a possible FM QCP. The above properties of $\text{A}_2\text{Cr}_3\text{As}_3$ suggest that these compounds are the possible solid-state analog of superfluid ^3He . Hence, further investigations of these compounds are important to bridge three large research areas: strong correlations, unconventional superconductivity, and topological quantum phenomena. Electronic structure calculations reveal that owing to 1D nature of the crystal structure, the band structures feature weak in-plane dispersions, and strong out-of-plane dispersions. The weak in-plane dispersion suffices to give a strong peak in the density-of-states, which is responsible for ferromagnetic fluctuations and spin-triplet superconductivity. There exists a quasi-three-dimensional Fermi surface (FS), and two quasi-one-dimensional FSs [18–20] which are strongly nested [21, 22]. The FS nesting opens a spin-fluctuation pairing channel in both spin-singlet and triplet channels. We computed the SC pairing symmetry in a three-band Hubbard model. We report that the lowest-energy pairing state lies in a novel spin-triplet channel with total spin $S_z = 0$, and the corresponding pairing symmetry is a $p_z = \sin k_z$ like. This gives a nodal line gap and is also orbital selective. The results are found to be consistent with the experimental data.

2. Experimental Details

The powder sample of $\text{Na}_2\text{Cr}_3\text{As}_3$ was prepared by the ion-exchange method with sodium naphthalene solution (Naph.- Na) in tetrahydrofuran (THF) using $\text{K}_2\text{Cr}_3\text{As}_3$ powder as the precursor [23]. Transverse field muon spin rotation (TF- μ SR) [24] measurements were carried

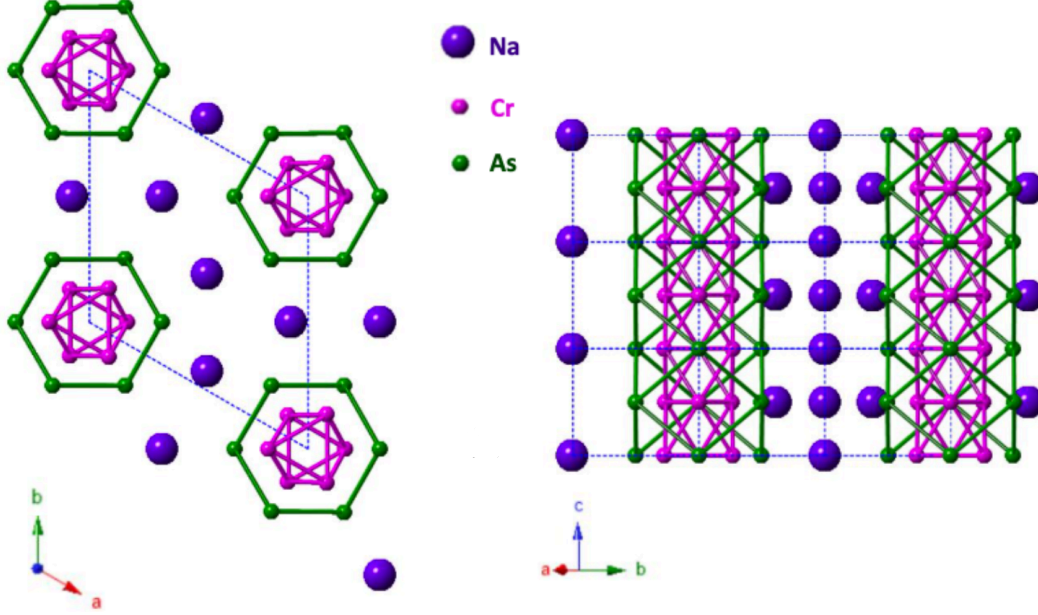


Figure 1: (Color online) The hexagonal lattice structure of $\text{Na}_2\text{Cr}_3\text{As}_3$. $\text{A}_2\text{Cr}_3\text{As}_3$ has a typical Q1D structure, which is derived from 1D CrAs chains that crystallize in the form of double-wall subnanotubes, with the alkali metal ions residing in the CrAs chains' interstitials.

out on the MUSR spectrometer at ISIS Facility, UK [25]. Small pieces (in pellet form) of $\text{Na}_2\text{Cr}_3\text{As}_3$ were mounted in sealed titanium (99.99 %) sample holder under He-exchange gas, which was placed in a He-3 system that has a temperature range of 0.3 K - 11 K. Using an active compensation system, the stray magnetic fields at the sample position were canceled to a level of 1 μT . TF- μSR measurements were performed in the superconducting mixed state in an applied field of 30 mT, well above the lower critical field of $H_{c1} \sim 2$ mT, but below the upper critical field of $H_{c2} \sim 54$ T of this material [26]. The TF- μSR data were collected in the field cooling mode, where the magnetic field 30 mT was applied at 11 K, above the superconducting transition T_C , and the sample was then cooled down to 0.3 K. The data were analyzed using the open software package WiMDA [27].

3. Results and discussion

3.1. Crystal structure and Magnetization

The crystal structure of $\text{Na}_2\text{Cr}_3\text{As}_3$ is shown in Fig. 1(a), which crystallizes in the hexagonal noncentrosymmetric structure with space group $P-6m2$ (No. 187), in which the $(\text{Cr}_3\text{As}_3)^{2-}$ linear chains are separated by Na^+ ions. Structurally, $\text{A}_2\text{Cr}_3\text{As}_3$ have a typical Q1D configuration originated from the 1D CrAs chains that crystallize in a fashion of double-wall subnanotubes, with the alkali metal ions located among the interstitials of the CrAs chains [26]. The upper critical field $\mu H_{c2}(0) \sim 54$ T exceed the Pauli paramagnetic limited $\mu H_p = 1.84 T_C \sim 16$ T [26], suggesting unconventional superconductivity in $\text{Na}_2\text{Cr}_3\text{As}_3$, which is also observed previously in $\text{A}_2\text{Cr}_3\text{As}_3$ ($\text{A}=\text{K}, \text{Rb}, \text{Cs}$) and ACr_3As_3 ($\text{A}=\text{K}$) superconductors [1]. Strong electron correlation effect is evident from large value of the Sommerfeld coefficient γ

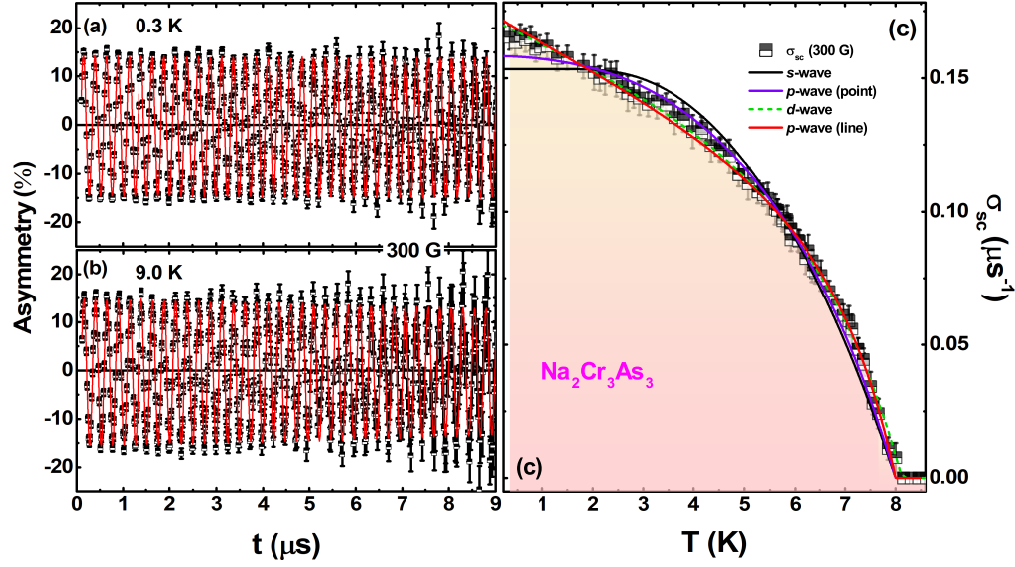


Figure 2: (Color online) The transverse field μ SR time spectra (one component) for $\text{Na}_2\text{Cr}_3\text{As}_3$ collected (a) at $T = 0.3$ K and (b) at $T = 9.0$ K in an applied magnetic field $H = 30$ mT in the field cooled (FC) state. (c) $\sigma_{sc}(T)$ of FC mode (symbols) and the lines are the fits to the data (see text). The black line shows the fit using an isotropic single-gap s -wave model with $2\Delta(0)/k_B T_C = 4.21$ ($\Delta(0) = 1.45(2)$ meV). The solid red line and green dot represent the fit to a p -wave and d -wave line gap model with $2\Delta(0)/k_B T_C = 9.14$ ($\Delta(0) = 3.15(6)$ meV) and $2\Delta(0)/k_B T_C = 6.44$ ($\Delta(0) = 2.22(4)$ meV) respectively. The shaded region covers the region of the nodal line fitting.

as 76.5 mJ/(mol-K²) in $\text{Na}_2\text{Cr}_3\text{As}_3$, this is a common feature in $\text{A}_2\text{Cr}_3\text{As}_3$ compounds due to reduced dimensionality [16]. In $\text{A}_2\text{Cr}_3\text{As}_3$ series, T_C increases dramatically from 2.2 to 8.0 K from Cs^+ to Na^+ indicating substantial positive chemical pressure effect on T_C and interchain coupling [?].

3.2. TF- μ SR analysis

To understand the enigmatic superconducting gap structure as proposed by the previous theoretical and experimental reports [11, 16], we have carried out the TF- μ SR study [28]. Figures 2 (a) and (b) show the TF- μ SR asymmetry-time spectra at 0.3 K ($\ll T_C$) and 9.0 K ($> T_C$) obtained in FC mode with an applied field of 30 mT ($H > H_{c1} \sim 2$ mT but below $H \ll H_{c2} \sim 54$ T). The observed decay of the μ SR signal with time below T_C is due to the inhomogeneous field distribution of the flux-line lattice. We have used an oscillatory decaying Gaussian function to fit the TF- μ SR asymmetry spectra, which is given below [29–33],

$$G_{z1}(t) = A_1 \cos(2\pi\nu_1 t + \theta) \exp\left(\frac{-\sigma^2 t^2}{2}\right) + A_2 \cos(2\pi\nu_2 t + \theta) \quad (1)$$

where A_i , ν_i and θ are the asymmetries, frequencies and initial phase angle of the muon precession signal from the sample ($i = 1$) and the background signal ($i = 2$) from the Ti-sample holder, respectively, with $\gamma_\mu/2\pi = 135.5$ MHz T⁻¹ is the muon gyromagnetic ratio. A_2 value is calculated from 0.3 K fitting data, θ values were kept zero. The total relaxation rate σ

contains two parts, superconducting vortex-lattice contributions (σ_{sc}) which is directly linked to the magnetic penetration depth λ_L and nuclear dipole moments (σ_{nm}). $\sigma_{nm} \sim 0.17 \mu s^{-1}$, is assumed to be constant over the entire temperature range between 0.3 K and 9 K, where $\sigma = \sqrt{(\sigma_{sc}^2 + \sigma_{nm}^2)}$. σ_{nm} is determined by fitting TF- μ SR above T_C . The lines in Fig. 2(a)-(b) illustrate the fits of the TF- μ SR data. The parameters A_2 and θ were estimated by fitting to the 0.3 K data and 9 K, respectively, and their values were kept fixed in the fitting between 0.3 K and 9 K. T_C derived from σ_{sc} data is ~ 8.0 K as shown in Fig. 2(c).

The magnetic penetration depth λ_L is related to σ_{sc} by the expression [34], $\sigma_{sc}^2/\gamma_\mu = 0.00371\Phi_0^2/\lambda_L^4$, where $\gamma_\mu/2\pi = 135.5$ MHz/T is the muon gyromagnetic ratio and $\Phi_0 = 2.068 \times 10^{-15}$ Wb is the magnetic-flux quantum, for a type-II superconductor with a large upper critical field and a hexagonal Abrikosov vortex lattice. $\lambda_L(T)$ is related to the superfluid density and can be used to determine the nature of the superconducting gap. The temperature dependence of $\sigma_{sc}(T)$ is shown in Figure 2(c). Below 1 K, it increases in a linear fashion. This non-constant low temperature behaviour is a hallmark of superconducting gap nodes. By analyzing the superfluid density data with different models of the gap function $\Delta_k(T)$, the pairing symmetry of Na₂Cr₃As₃ can be understood. We calculate the superfluid density for a given pairing model as follows [?, 35]:

$$\frac{\sigma_{sc}(T)}{\sigma_{sc}(0)} = \frac{\lambda_L^{-2}(T)}{\lambda_L^{-2}(0)} = 1 + 2 \left\langle \int_{\Delta_k(T)}^{\infty} \frac{E}{\sqrt{E^2 - |\Delta_k(T)|^2}} \frac{\partial f}{\partial E} dE \right\rangle_{FS} \quad (2)$$

where $f = [1 + \exp(\frac{E}{k_B T})]^{-1}$ is the Fermi function and $\langle \rangle_{FS}$ represents the Fermi surface's average (assumed to be spherical). We take $\Delta_k(T) = \Delta(T)g_k$ where we assume a temperature dependence that is universal $\Delta(T) = \Delta_0 \tanh[1.82\{1.018(T_C/T - 1)\}^{0.51}]$. The magnitude of the gap at 0 K is Δ_0 , and the function g_k denotes the gap's angular dependence [?, 35] and is given for the various models in Table I [36–38].

We have analyzed the temperature dependence of σ_{sc} based on different models (isotropic s -wave, nodal d -wave, p -wave line node, and p -wave point node) as shown in Fig. 2(c). The fit to $\sigma_{sc}(T)$ data of Na₂Cr₃As₃ gives $2\Delta(0)/k_B T_C = 4.21$ for a single isotropic s -wave and a larger value of $2\Delta(0)/k_B T_C = 9.14$ for a p -wave line node supporting p_z pairing and $2\Delta(0)/k_B T_C = 6.44$ ($\Delta(0) = 2.22(4)$ meV) for a d -wave line node. The observed $2\Delta(0)/k_B T_C$ values are consistent with those found in other compounds in this family [13]. The TF- μ SR data suggests the presence of line nodes in the superconducting energy gap. The TF- μ SR results of (K,Cs)₂Cr₃As₃ [13], also support the presence of line nodes in the superconducting gap. Furthermore, the large gap value obtained from the nodal p -wave fit is much larger than the gap value expected for BCS superconductors (3.53), indicates the presence of strong coupling superconductivity, which is in line with the observed gap values found in (K,Cs)₂Cr₃As₃ [13]. The observed gap symmetry in Na₂Cr₃As₃ together with ⁷⁵As nuclear quadrupole resonance and theoretical calculations [16] in A₂Cr₃As₃ suggest unconventional pairing mechanism in (Na,K,Rb,Cs)₂Cr₃As₃. A summary of the different gap symmetries were used to fit the magnetic penetration depth for Na₂Cr₃As₃ is shown in Table I. Furthermore, from our TF- μ SR data we have estimated the magnetic penetration depth $\lambda_L(0)$, superconducting carrier density n_s , and effective-mass enhancement m^* to be $\lambda_L(0) = 790(4)$ nm (from the nodal p -wave fit), $n_s = 8.5(1) \times 10^{26}$ carriers/m³, and $m^* = 1.884(3) m_e$, respectively. A₂Cr₃As₃ family is known for having a large magnetic penetration depth [13]. This is due to the strong interaction that

Table 1: A summary of the different gap symmetries were

used to fit the magnetic penetration depth in Figure 2 for Na₂Cr₃As₃ with $T_C \sim 8.0$ K. The first column corresponds to the models in the figure, g_k gives the angular dependence of the gap and $2\Delta(0)/k_B T_C$ is the gap magnitude in the calculation that best fitted the data.

Pairing state	g_k	Gap $\Delta(0)$ (meV)	Gap Ratio $2\Delta(0)/k_B T_C$
<i>s</i> -wave	1	1.45(2)	4.21
<i>d</i> -wave (line)	$\cos 2\phi$	2.22(4)	6.44
<i>p</i> -wave (point)	$\sin \theta$	1.80(3)	5.22
<i>p</i> -wave (line)	$\cos \theta$	3.15(6)	9.14

occurs as a result of the quasi-one-dimensional structure. For K₂Cr₃As₃, $\lambda_L(0) = 646$ nm, Cs₂Cr₃As₃, $\lambda_L(0) = 954$ nm [13].

4. Theoretical Calculations

Earlier electronic structure calculations have shown that the low-energy properties are defined by a minimal three-band model, stemming mainly from the d_{z^2} , d_{xy} , and $d_{x^2-y^2}$ orbitals of the Cr-atoms [39–42]. We adopt the three-band tight-binding model from Ref. [40]. The corresponding Fermi surfaces (FSs) are shown in Fig. 3(a), with a gradient color denoting the corresponding orbital weight. Interestingly, there lie two flat FS sheets at constant k_z cuts which have weak basal plane anisotropy. Such FSs govern strong peaks in the density of state (DOS) at the Fermi level, and hence ferromagnetic fluctuations. In addition, due to the separation of the flat FS sheets between the nearly constant $\pm k_z^*$ direction, there arises strong FS nestings around $\mathbf{Q} \rightarrow (0, 0, Q_z)$, where $Q_z = 2k_z^*$. Such a nesting promotes magnetic fluctuation mediated pairing channel which follows the relation $\text{sgn}[\Delta_{\mathbf{k}}] = -\text{sgn}[\Delta_{\mathbf{k}+\mathbf{Q}}]$. Through numerical calculation, we show below that the pairing symmetry turns out to be p_z in nature with triplet pairing channel but for $S = 0$. We notice that the FS topology of this material is qualitatively similar to the iso-structural heavy-fermion superconductor UPt₃ [43, 44] in which also unconventional p -wave pairing symmetry due to FM fluctuation has been discussed before. [44, 45]

We compute the pairing state $\Delta_{\mathbf{k}}$ as the eigenfunction of the leading eigenvalue of the spin-fluctuation mediated pairing interaction $\tilde{\Gamma}_{\uparrow\uparrow}(\mathbf{k} - \mathbf{k}')$ by solving the following equation:

$$\Delta(\mathbf{k}) = -\lambda \frac{1}{\Omega_{\text{BZ}}} \sum_{\mathbf{k}'} \Gamma_{\uparrow\downarrow}(\mathbf{k} - \mathbf{k}') \Delta(\mathbf{k}'). \quad (3)$$

Ω_{BZ} denote the Brillouin zone volume. λ is the pairing eigenvalue (proportional to the SC coupling strength), and $\Delta(\mathbf{k})$ is the corresponding pairing eigenfunction. For the calculation of $\tilde{\Gamma}_{\uparrow\uparrow}(\mathbf{k} - \mathbf{k}')$, we consider a three-band Hubbard model with intra-, inter-orbital Hubbard interactions, Hund's coupling, and pair-hopping terms. Then, we obtain the pairing potential by considering the bubble and ladder diagrams: [46–68]

$$\tilde{\Gamma}_{\uparrow\downarrow}(\mathbf{q}) = \frac{1}{2} [3\tilde{U}_s \tilde{\chi}_s(\mathbf{q}) \tilde{U}_s - \tilde{U}_c \tilde{\chi}_c(\mathbf{q}) \tilde{U}_c + \tilde{U}_s + \tilde{U}_c]. \quad (4)$$

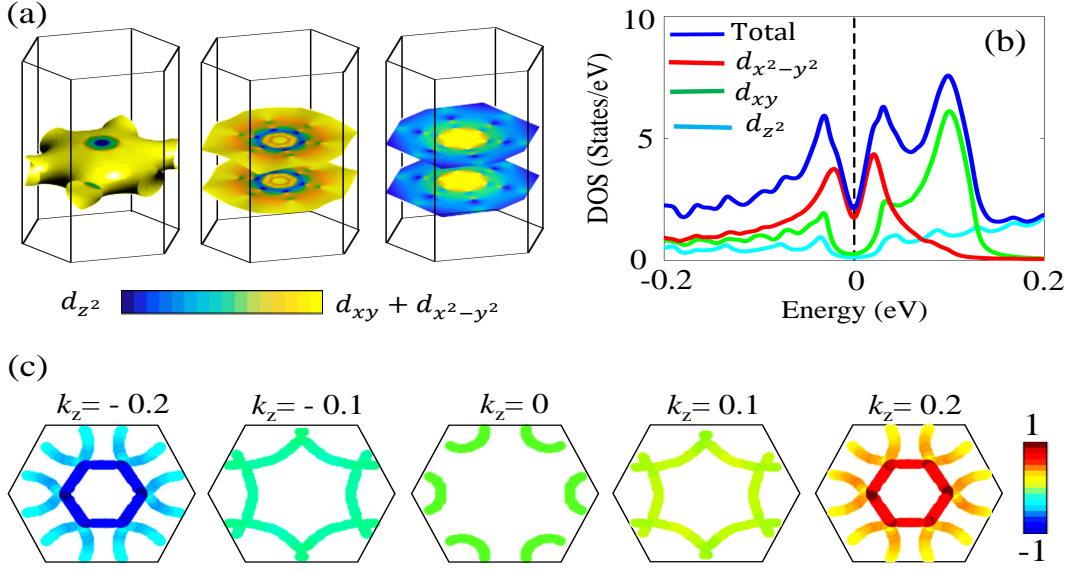


Figure 3: Theoretical results. (a) Three FS sheets are plotted separately for visualization. The blue to yellow colormap gives the orbital weight (see colorbar). (b) DOS in the SC state is plotted near the Fermi level. We have used an artificially large SC gap of 30 meV for visualization. Finite DOS at the Fermi level is an artifact due to finite broadening for numerical convergence. Blue color gives the total DOS, while other colors give orbital resolved DOS. (c) 2D FS cuts in various representative constant values of k_z . The red to blue color gradient paints the corresponding pairing eigenstate $\Delta(\mathbf{k})$ as calculated by using Eq. 8 in SM.

Here we only present the results for the spin-flip component of the pairing potential, while the pairing with finite spin components ($\tilde{\Gamma}_{\uparrow\uparrow}/\tilde{\Gamma}_{\downarrow\downarrow}$) are also considered but found to be much lower in strength. This is consistent with the absence of a finite magnetic moment in the muon experimental data. The symbol ‘tilde’ denotes a tensor in the orbital basis. The subscripts ‘s’ and ‘c’ denote spin and charge density-density fluctuation channels, respectively. $\tilde{\chi}_{s/c}$ are the spin and charge density-density correlation functions (tensors in the same orbital basis), computed within the random-phase-approximation (RPA). The details of the formalism is given in SM. $\tilde{U}_{s/c}$ are the onsite interaction tensors for spin and charge fluctuations, respectively whose non-vanishing components are the nonzero components of the matrices \tilde{U}_c and \tilde{U}_s are given as [69]: $(\tilde{U}_{s,c})_{\alpha\alpha}^{\alpha\alpha} = U_\alpha$, $(\tilde{U}_s)_{\beta\beta}^{\alpha\alpha} = \frac{1}{2}J_H$, $(\tilde{U}_c)_{\beta\beta}^{\alpha\alpha} = 2V - J_H$, $(\tilde{U}_s)_{\alpha\beta}^{\alpha\beta} = V$, $(\tilde{U}_c)_{\alpha\beta}^{\alpha\beta} = -V + 3J_H$, $(\tilde{U}_{s,c})_{\alpha\beta}^{\beta\alpha} = J'$. α, β are orbital indices. The intra-orbital Hubbard interaction for the three orbitals are $U_m = 400, 200, 200$ meV, the inter-orbital interaction is $V = 150$ meV, and Hund’s coupling and pair-hopping interactions are $J_H = J' = 50$ meV. These values are deduced from the Kanamori criterion and the pairing eigenfunctions do not change with the parameter values, while the pairing interaction increases with increasing interactions.

The interplay between FS topology, nesting, and pairing symmetry can be understood as follows. For repulsive interaction and $\lambda > 0$ in Eq. 3, the pairing eigenstate $\Delta(\mathbf{k})$ must change *sign* over the FS to compensate for the negative sign in the left hand side of Eq. 2. $\Delta(\mathbf{k})$ changes sign between \mathbf{k} and \mathbf{k}' which may be in a given band or between different bands. These

two momenta are connected by the nesting feature at $\mathbf{q} = \mathbf{k} - \mathbf{k}'$ at which $\Gamma_{\uparrow/\downarrow}(\mathbf{q})$ acquires strong peaks. The loci of the peaks in $\Gamma'_{\nu\nu'}(\mathbf{q})$ is primarily dictated by the FS nesting, while the overall amplitude is determined by the interaction strength.

We solve Eq. 3 for the three FSs plotted on in Fig. 3(a). Our direct eigenvalue and eigenfunction solver yields the higher eigenvalue to be $\lambda \sim 0.1$ and the corresponding eigenfunction gives a $p_z = \sin(k_z)$ symmetry. We plot the eigenfunction as a color gradient map on several representative FS cuts in Fig. 3(c). We find that the gap $\Delta(\mathbf{k})$ is odd under the Mirror symmetry along the k_z -direction, and changes sign between $\pm k_z$. There is a slight in-plane anisotropy on the gap, but not significant enough to promote sign-reversal in the k_x, k_y plane. This particular pairing symmetry is consistent with the nesting properties between the two flat FS sheets across $\pm k_z^*$ as discussed above. The same pairing state is obtained in previous calculations in this family of materials and is also obtained in UPt_3 superconductor [39, 40].

The p_z pairing symmetry being odd in parity is consistent with a spin-triplet Cooper pair. Among the three spin-triplet channels, the spin-flip term $1/\sqrt{2}(\uparrow\downarrow + \downarrow\uparrow)$ does not induce any spin-polarization. This is also the pairing channel we find to be dominant compared to the spin-polarized channels. Therefore, despite the time-reversal symmetry breaking, this state does not induce any magnetic moment, and thus the time-reversal breaking is not detectable in the muon experiment. This result is consistent with our zero-field μ SR on $\text{Na}_2\text{Cr}_3\text{As}_3$ measurements.

The obtained p_z pairing channel gives a nodal line gap on the $k_z = 0$ FS cut, as shown in the middle plot in Fig. 3(c). The corresponding nodal structure appears in a ‘V’ shape DOS shown in Fig. 3(b) by the blue line. We also split the contributions to the DOS from three different orbitals, as shown in different colors. We notice that since the FS near the $k_z = 0$ region is dominated by mainly the $d_{x^2-y^2}$ orbital, the nodal structure is mainly obtained in this orbital, while the other two orbitals see very much fully gapped behavior. Given that the total DOS has a ‘V’-shave behavior, the low-temperature dependence of the superfluid density acquires a linear-in- T dependence as seen experimentally.

5. Conclusions

In summary, we have presented TF- μ SR result in the superconducting state of $\text{Na}_2\text{Cr}_3\text{As}_3$, which has a Q1D noncentrosymmetric crystal structure. The temperature dependence of magnetic penetration depth obtained from the TF- μ SR results support the p -wave line node symmetry fitted well with the observed ^{75}As nuclear quadrupole resonance data. Despite a p -wave, triplet pairing state, we do not find any evidence of a magnetic moment of the Cooper pair. These results are consistent with the theoretical calculation. The theory is developed for a three-band Hubbard model and the pairing potential is obtained through many-body effects. We find that the lowest energy state of superconductivity is a spin-triplet p -wave, but in the $S_z = 0$ channel. The corresponding pairing state possesses a p_z symmetry which changes sign across the $k_z = 0$ mirror plane and stems from the FS nesting between quasi-flat FS sheets lying at some $\pm k_z$ planes. Such a spin-zero triplet p -wave pairing channel is a novel pairing state which can be potentially important for chiral superconductivity and topological phases.

$$S_z = +1 : c_{k,\uparrow}c_{-k,\uparrow} \quad (5)$$

$$S_z = -1 : c_{k,\downarrow}c_{-k,\downarrow} \quad (6)$$

$$S_z = 0 : (c_{k,\uparrow}c_{-k,\downarrow} + c_{k,\downarrow}c_{-k,\uparrow})/\sqrt{2} \quad (7)$$

One may wonder a $S_z = 0$, nodal gap can also arise from a spin-singlet, d -wave (or similar even parity) channel [70, 71]. From the experimental fits to penetration depth data, it is difficult to pin down a particular momentum structure of the gap. For that, the ARPES, or inelastic neutron scattering, or quasiparticle interference (QPI) pattern, or magnetic field angle dependent specific heat or thermal conductivity data are required. However, theoretically since we find only one robust pairing symmetry, and other pairing solutions have much lower coupling strength (and hence much higher total energy), we are confident that the future momentum-resolved experiments will affirm the $\sin(k_z)$ structure of the gap symmetry.

Acknowledgments

A.B. would like to acknowledge financial support from the Department of Science and Technology, India (SR/NM/Z-07/2015) for the financial support and Jawaharlal Nehru Centre for Advanced Scientific Research (JNCASR) for managing the project. and the Department of Science and Technology (DST) India for Inspire Faculty Research Grant (DST/INSPIRE/04/2015/000169). D. T. A. would like to acknowledge funding support the Royal Society of London for UK-China Newton mobility grant, Newton Advanced Fellowship funding and JSPS for an invitation fellowship. T.D.'s research is supported by the STARS-MHRD research fund (STARS/APR2019/PS/156/FS). The work at Fudan University was supported by the Innovation Program of Shanghai Municipal Education Commission (Grant No. 2017-01-07-00-07-E00018) and the National Natural Science Foundation of China (Grant No.11874119). D.D. would like to thank Andreas Suter for fruitful discussion.

Supplemental Material

Supplemental Material: μ SR study of unconventional pairing symmetry in the quasi-1D $\text{Na}_2\text{Cr}_3\text{As}_3$ superconductor

The interaction Hamiltonian is modeled within the onsite Hubbard interactions including intra-orbital interaction (U_m), inter-orbital interaction (V), Hund's coupling (J_H), and pair-hopping interaction J' :

$$\begin{aligned} H_{\text{int}} = & \sum_{\mathbf{k}_1 - \mathbf{k}_4} [\sum_{\alpha} U_{\alpha} c_{\mathbf{k}_1, \alpha \uparrow}^{\dagger} c_{\mathbf{k}_2, \alpha \uparrow} c_{\mathbf{k}_3, \alpha \downarrow}^{\dagger} c_{\mathbf{k}_4, \alpha \downarrow} \\ & + \sum_{\alpha < \beta, \sigma} (V c_{\mathbf{k}_1, \alpha \sigma}^{\dagger} c_{\mathbf{k}_2, \alpha \sigma} c_{\mathbf{k}_3, \beta \bar{\sigma}}^{\dagger} c_{\mathbf{k}_4, \beta \bar{\sigma}} + (V - J_H) c_{\mathbf{k}_1, \alpha \sigma}^{\dagger} c_{\mathbf{k}_2, \alpha \sigma} c_{\mathbf{k}_3, \beta \sigma}^{\dagger} c_{\mathbf{k}_4, \beta \sigma}) \\ & + \sum_{\alpha < \beta, \sigma} (J_H c_{\mathbf{k}_1, \alpha \sigma}^{\dagger} c_{\mathbf{k}_3, \beta \bar{\sigma}}^{\dagger} c_{\mathbf{k}_2, \alpha \bar{\sigma}} c_{\mathbf{k}_4, \beta \sigma} + J' c_{\mathbf{k}_1, \alpha \sigma}^{\dagger} c_{\mathbf{k}_3, \alpha \bar{\sigma}}^{\dagger} c_{\mathbf{k}_2, \beta \bar{\sigma}} c_{\mathbf{k}_4, \beta \sigma} + h.c.)]. \end{aligned} \quad (8)$$

Here $c_{\mathbf{k}_1, \alpha \sigma}^{\dagger}$ ($c_{\mathbf{k}_1, \alpha \sigma}$) is the creation (annihilation) operator for an orbital α at crystal momentum \mathbf{k}_1 with spin $\sigma = \uparrow$ or \downarrow , where $\bar{\sigma}$ corresponds to opposite spin of σ . In the multiorbital spinor, the above interacting Hamiltonian can be collected in a interaction tensor $\tilde{U}_{s/c}$, where the subscripts s, c stand spin and charge density fluctuations. The nonzero components of the matrices \tilde{U}_c and \tilde{U}_s are given in the main text.

Of course, it is implicit that all the interaction parameters are orbital dependent. Within the RPA, spin and charge channels become decoupled. The collective many-body corrections of the density-fluctuation spectrum can be written in matrix representation: $\tilde{\chi}_{s/c} = \tilde{\chi}^0 [\tilde{I} \mp \tilde{U}_{s/c} \tilde{\chi}^0]^{-1}$, for spin and charge densities, respectively. $\tilde{\chi}^0$ matrix consists of components $\chi_{0,mn}^{st}$ with the same basis in which the interactions $\tilde{U}_{s/c}$ are defined above.

By expanding the interaction term to multiple interaction channels, and collecting the terms which give a pairing interaction (both singlet and triplet channels are considered) we obtain the effective pairing potential $\Gamma_{\alpha\beta}^{\gamma\delta}(\mathbf{q})$ as [46–68]

$$H_{\text{int}} \approx \frac{1}{\Omega_{\text{BZ}}^2} \sum_{\alpha\beta\gamma\delta} \sum_{\mathbf{k}\mathbf{q},\sigma\sigma'} \Gamma_{\alpha\beta}^{\gamma\delta}(\mathbf{q}) \times c_{\alpha\sigma}^\dagger(\mathbf{k}) c_{\beta\sigma'}^\dagger(-\mathbf{k}) c_{\gamma\sigma'}(-\mathbf{k} - \mathbf{q}) c_{\delta\sigma}(\mathbf{k} + \mathbf{q}). \quad (9)$$

$\sigma' = \pm\sigma$ give triplet and singlet pairing channels, respectively. This pairing potential, obtained in Refs. [66], includes a summation of bubble and ladder diagrams within the random phase approximation (RPA). The pairing potential in general involves four orbital indices and thus is a tensor in the orbital basis. We denote all such tensors by the ‘tilde’ symbol. The pairing potentials in the singlet ($\tilde{\Gamma}_{\uparrow\downarrow}$) and triplet ($\tilde{\Gamma}_{\uparrow\uparrow}$) channels are

$$\tilde{\Gamma}_{\uparrow\downarrow}(\mathbf{q}) = \frac{1}{2} [3\tilde{U}_s \tilde{\chi}_s(\mathbf{q}) \tilde{U}_s - \tilde{U}_c \tilde{\chi}_c(\mathbf{q}) \tilde{U}_c + \tilde{U}_s + \tilde{U}_c], \quad (10)$$

$$\tilde{\Gamma}_{\uparrow\uparrow/\downarrow\downarrow}(\mathbf{q}) = -\frac{1}{2} [\tilde{U}_s \tilde{\chi}_s(\mathbf{q}) \tilde{U}_s + \tilde{U}_c \tilde{\chi}_c(\mathbf{q}) \tilde{U}_c - \tilde{U}_s - \tilde{U}_c]. \quad (11)$$

Here subscript ‘s’ and ‘c’ denote spin and charge fluctuation channels, respectively. $\tilde{U}_{s/c}$ are the onsite interaction tensors for spin and charge fluctuations, respectively, defined in the same basis as $\tilde{\Gamma}$. Its non-vanishing components are given in the main text.

$\tilde{\chi}_{s/c}$ are the density-density correlators (tensors in the same orbital basis) for the spin and charge density channels. We define the non-interacting density-density correlation function (Lindhard susceptibility) $\tilde{\chi}_0$ within the standard linear response theory:

$$[\chi_0(\mathbf{q})]_{\alpha\beta}^{\gamma\delta} = -\frac{1}{\Omega_{\text{BZ}}} \sum_{\mathbf{k},\nu\nu'} \phi_{\beta}^{\nu}(\mathbf{k}) \phi_{\alpha}^{\nu*}(\mathbf{k}) \phi_{\delta}^{\nu'}(\mathbf{k} + \mathbf{q}) \phi_{\gamma}^{\nu'*}(\mathbf{k} + \mathbf{q}) \times \frac{f(E_{\nu'}(\mathbf{k} + \mathbf{q})) - f(E_{\nu}(\mathbf{k}))}{E_{\nu'}(\mathbf{k} + \mathbf{q}) - E_{\nu}(\mathbf{k}) + i\epsilon}. \quad (12)$$

$E_{\nu}(\mathbf{k})$ are the eigenvalues of the two Wannier orbital Hamiltonians and $\phi_{\alpha}^{\nu}(\mathbf{k})$ gives a component of the eigenvector. f is the Fermi distributions function. Many body effect of Coulomb interaction in the density-density correlation is captured within S -matrix expansion of Hubbard Hamiltonian in Eq. 9. By summing over different bubble and ladder diagrams we obtain the RPA spin and charge susceptibilities as:

$$\tilde{\chi}_{s/c}(\mathbf{q}) = \tilde{\chi}_0(\mathbf{q}) (\tilde{I} \mp \tilde{U}_{s/c} \tilde{\chi}_0(\mathbf{q}))^{-1}, \quad (13)$$

where \tilde{I} is the unit matrix.

Eq. 9 gives the pairing interaction for pairing between orbitals. However, we solve the BCS gap equation in the band basis. To make this transformation, we make use of the unitary transformation $c_{\alpha\sigma} \rightarrow \sum_{\nu} \mathcal{U}_{\nu}^{\alpha} \gamma_{\nu\sigma}$ for all \mathbf{k} and spin σ . With this substitution we obtain the pairing interaction Hamiltonian in the band basis as

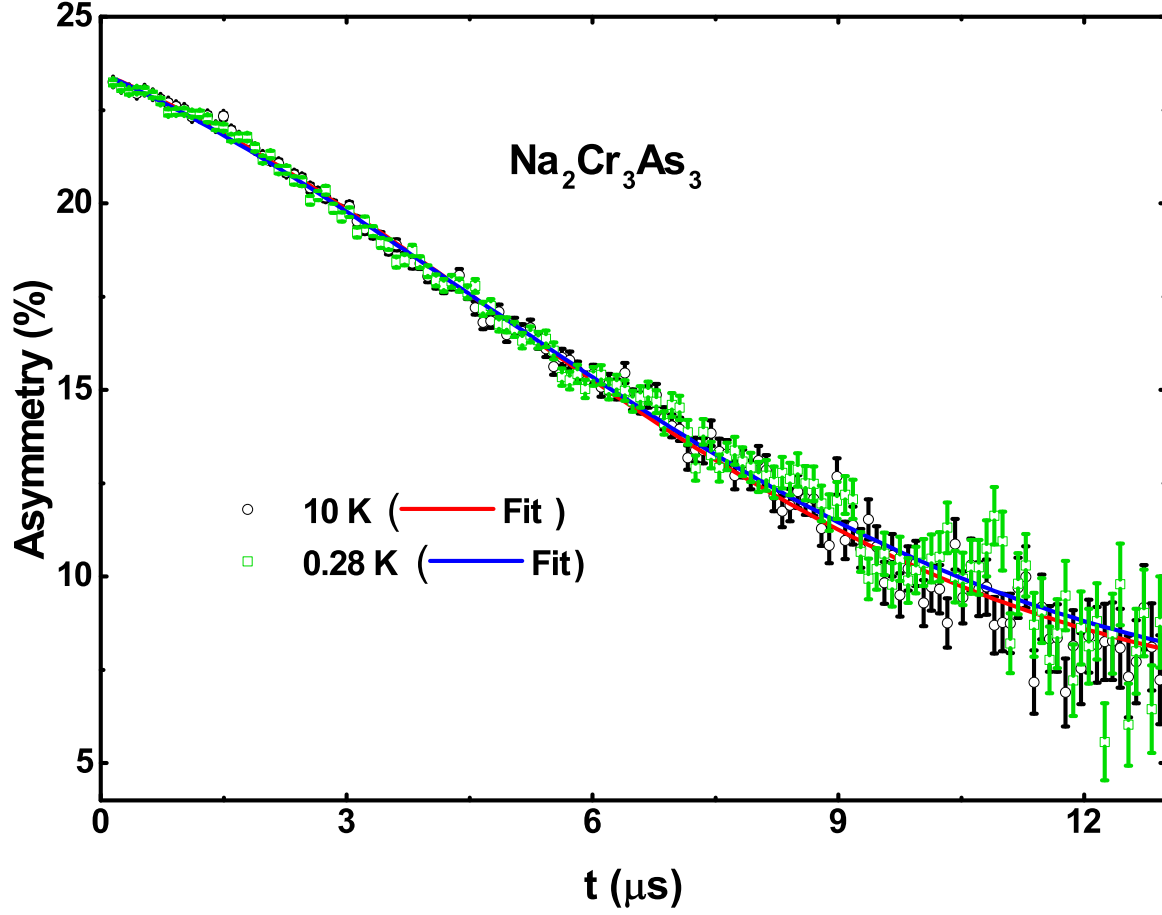


Figure 4: Zero field μ SR time spectra for $\text{Na}_2\text{Cr}_3\text{As}_3$ collected at 0.28 K (green square) and 10 K (black circle) are shown together with lines that are least square fit to delta.

$$H_{\text{int}} \approx \sum_{\nu\nu'} \sum_{\mathbf{k}\mathbf{q},\sigma\sigma'} \Gamma'_{\nu\nu'}(\mathbf{k}, \mathbf{q}) \times \frac{1}{\Omega_{\text{BZ}}^2} \gamma_{\nu\sigma}^\dagger(\mathbf{k}) \gamma_{\nu\sigma'}^\dagger(-\mathbf{k}) \gamma_{\nu'\sigma'}(-\mathbf{k} - \mathbf{q}) \gamma_{\nu'\sigma}(\mathbf{k} + \mathbf{q}). \quad (14)$$

The same equation holds for both singlet and triplet pairing and thus henceforth we drop the corresponding symbol for simplicity. The band pairing interaction $\Gamma'_{\nu\nu'}$ is related to the corresponding orbital one as $\Gamma'_{\nu\nu'}(\mathbf{k}, \mathbf{q}) = \sum_{\alpha\beta\gamma\delta} \Gamma_{\alpha\beta}^{\gamma\delta}(\mathbf{q}) \phi_\alpha^{\nu\dagger}(\mathbf{k}) \phi_\beta^{\nu\dagger}(-\mathbf{k}) \phi_\gamma^{\nu'}(-\mathbf{k} - \mathbf{q}) \phi_\delta^{\nu'}(\mathbf{k} + \mathbf{q})$. We define the SC gap in the ν^{th} -band as

$$\Delta_\nu(\mathbf{k}) = -\frac{1}{\Omega_{\text{BZ}}} \sum_{\nu',\mathbf{q}} \Gamma'_{\nu\nu'}(\mathbf{k}, \mathbf{q}) \langle \gamma_{\nu'\sigma'}(-\mathbf{k} - \mathbf{q}) \gamma_{\nu'\sigma}(\mathbf{k} + \mathbf{q}) \rangle, \quad (15)$$

where the expectation value is taken over the BCS ground state. In the limit $T \rightarrow 0$ we have $\langle \gamma_{\nu\sigma}(-\mathbf{k}) \gamma_{\nu\sigma}(\mathbf{k}) \rangle \rightarrow \lambda \Delta_\nu(\mathbf{k})$, with λ is the SC coupling constant. Substituting this in Eq. 15, we get

$$\Delta_\nu(\mathbf{k}) = -\lambda \frac{1}{\Omega_{\text{BZ}}} \sum_{\nu',\mathbf{q}} \Gamma'_{\nu\nu'}(\mathbf{k}, \mathbf{q}) \Delta_{\nu'}(\mathbf{k} + \mathbf{q}). \quad (16)$$

This is an eigenvalue equation of the pairing potential $\Gamma'_{\nu\nu'}(\mathbf{q} = \mathbf{k} - \mathbf{k}')$ with eigenvalue λ and eigenfunction $\Delta_\nu(\mathbf{k})$. The \mathbf{k} -dependence of $\Delta_\nu(\mathbf{k})$ dictates the pairing symmetry for a given eigenvalue. While there are many solutions (as many as the \mathbf{k} -grid), however, we consider the highest eigenvalue since this pairing symmetry can be shown to have the lowest Free energy value in the SC state [66].

Zero Field μ SR: ZF- μ SR were used to check for the presence of any hidden magnetic ordering in $\text{Na}_2\text{Cr}_3\text{As}_3$. Fig. 4 compares the zero field time-dependent asymmetry spectra above and below and T_C (for $T = 0.28$ K and 10.0 K). The ZF- μ SR data can be well described using a damped Gaussian Kubo-Toyabe (KT) function [72],

$$G_{z2}(t) = A_3 G_{KT}(t) e^{-\lambda_\mu t} + A_{bg}, \quad (17)$$

where $G_{KT}(t) = [\frac{1}{3} + \frac{2}{3}(1 - \sigma_{KT}^2 t^2) \exp(-\frac{\sigma_{KT}^2 t^2}{2})]$, is known as the Gaussian Kubo-Toyabe function, A_3 is the zero field asymmetry of the sample signal, A_{bg} is the background signal, σ_{KT} and λ_μ are the muon spin relaxation rates due to randomly oriented nuclear moments (the local field distribution width $H_\mu = \sigma/\gamma_\mu$, with muon gyromagnetic ratio $\gamma_\mu/2\pi = 135.53$ MHz/T. No sign of muon spin precession is visible either at 0.28 K or 10 K, ruling out the presence of large internal field as seen in magnetically ordered systems. The only possibility is that the muon spin relaxation is due to static, randomly oriented local fields associated with the electronic and nuclear moments at the muon site. There is no evidence of time-reversal symmetry breaking in $\text{Na}_2\text{Cr}_3\text{As}_3$.

Fits to the ZF- μ SR asymmetry data using Eq. 17 and shown by the solid lines in Fig. 4 give $\sigma_{KT} = 0.094 \mu\text{s}^{-1}$ and $\lambda_\mu = 0.057 \mu\text{s}^{-1}$ at 10 K and $\sigma_{KT} = 0.098 \mu\text{s}^{-1}$ and $\lambda_\mu = 0.053 \mu\text{s}^{-1}$ at 0.28 K.

References

- [1] Mackenzie A P and Maeno Y 2003 *Reviews of Modern Physics* **75** 657
- [2] Xu Y, Sheng Y and Yang Y f 2019 *Physical review letters* **123** 217002
- [3] Huxley A, Sheikin I, Ressouche E, Kernavanois N, Braithwaite D, Calemczuk R and Flouquet J 2001 *Physical Review B* **63** 144519
- [4] Tou H, Kitaoka Y, Ishida K, Asayama K, Kimura N, Yamamoto E, Haga Y, Maezawa K *et al.* 1998 *Physical review letters* **80** 3129
- [5] Wu W, Cheng J, Matsubayashi K, Kong P, Lin F, Jin C, Wang N, Uwatoko Y and Luo J 2014 *Nature communications* **5** 1–5
- [6] Dai P, Mook H A, Hayden S M, Aeppli G, Perring T G, Hunt R D and Doğan F 1999 *Science* **284** 1344–1347
- [7] Dai P 2015 *Reviews of Modern Physics* **87** 855
- [8] Allan M, Massee F, Morr D, Van Dyke J, Rost A, Mackenzie A, Petrovic C and Davis J 2013 *Nature physics* **9** 468–473
- [9] Varoquaux E 2015 *Reviews of Modern Physics* **87** 803
- [10] Bao J K, Liu J Y, Ma C W, Meng Z H, Tang Z T, Sun Y L, Zhai H F, Jiang H, Bai H, Feng C M *et al.* 2015 *Physical Review X* **5** 011013
- [11] Wu X, Yang F, Le C, Fan H and Hu J 2015 *Physical Review B* **92** 104511
- [12] Pang G, Smidman M, Jiang W, Bao J, Weng Z, Wang Y, Jiao L, Zhang J, Cao G and Yuan H 2015 *Physical Review B* **91** 220502
- [13] Adroja D, Bhattacharyya A, Telling M, Feng Y, Smidman M, Pan B, Zhao J, Hillier A, Pratt F and Strydom A 2015 *Physical Review B* **92** 134505

- [14] Adroja D, Bhattacharyya A, Smidman M, Hillier A, Feng Y, Pan B, Zhao J, Lees M R, Strydom A and Biswas P K 2017 *Journal of the Physical Society of Japan* **86** 044710
- [15] Tang Z T, Bao J K, Liu Y, Sun Y L, Ablimit A, Zhai H F, Jiang H, Feng C M, Xu Z A and Cao G H 2015 *Physical Review B* **91** 020506
- [16] Luo J, Yang J, Zhou R, Mu Q, Liu T, Ren Z a, Yi C, Shi Y and Zheng G q 2019 *Physical review letters* **123** 047001
- [17] Taddei K M, Xing G, Sun J, Fu Y, Li Y, Zheng Q, Sefat A S, Singh D J and de la Cruz C 2018 *Physical review letters* **121** 187002
- [18] Jiang H, Cao G and Cao C 2015 *Scientific reports* **5** 1–6
- [19] Alemany P and Canadell E 2015 *Inorganic chemistry* **54** 8029–8034
- [20] Subedi A 2015 *Physical Review B* **92** 174501
- [21] Wu X, Yang F, Le C, Fan H and Hu J 2015 *Physical Review B* **92** 104511
- [22] Zhong H, Feng X Y, Chen H and Dai J 2015 *Physical review letters* **115** 227001
- [23] Tang Z T, Bao J K, Wang Z, Bai H, Jiang H, Liu Y, Zhai H F, Feng C M, Xu Z A and Cao G H 2015 *Science China Materials* **58** 16–20
- [24] Sonier J E, Brewer J H and Kiefl R F 2000 *Reviews of Modern Physics* **72** 769
- [25] Lee S L, Cywinski R and Kilcoyne S 1999 *Muon science: Muons in physics, chemistry and materials* vol 51 (CRC press)
- [26] Mu Q G, Ruan B B, Pan B J, Liu T, Yu J, Zhao K, Chen G F and Ren Z A 2018 *Physical Review Materials* **2** 034803
- [27] Pratt F 2000 *Physica B: Condensed Matter* **289** 710–714
- [28] Bhattacharyya A and et al 2018 Investigation of superconducting ground state of quasi-one-dimensional superconductor $\text{Na}_2\text{Cr}_3\text{As}_3$: A μ SR study URL <https://doi.org/10.5286/ISIS.E.RB1820141>
- [29] Bhattacharyya A, Ferreira P, Santos F, Adroja D, Lord J, Correa L, Machado A, Manesco A and Eleno L T 2020 *Physical Review Research* **2** 022001
- [30] Bhattacharyya A, Rodiere P, Vaney J B, Biswas P, Hillier A, Bosin A, Bernardini F, Tencé S, Adroja D and Cano A 2020 *Physical Review B* **101** 224502
- [31] Bhattacharyya A, Adroja D, Smidman M and Anand V 2018 *Science China Physics, Mechanics & Astronomy* **61** 1–22
- [32] Bhattacharyya A, Adroja D, Panda K, Saha S, Das T, Machado A, Cigarroa O, Grant T, Fisk Z, Hillier A et al. 2019 *Physical review letters* **122** 147001
- [33] Panda K, Bhattacharyya A, Adroja D, Kase N, Biswas P, Saha S, Das T, Lees M and Hillier A 2019 *Physical Review B* **99** 174513
- [34] Brandt E H 2003 *Physical Review B* **68** 054506
- [35] Carrington A and Manzano F 2003 *Physica C: Superconductivity* **385** 205–214
- [36] Prozorov R and Giannetta R W 2006 *Superconductor Science and Technology* **19** R41
- [37] Pang G, Smidman M, Jiang W, Bao J, Weng Z, Wang Y, Jiao L, Zhang J, Cao G and Yuan H 2015 *Physical Review B* **91** 220502
- [38] Ozaki M a, Machida K and Ohmi T 1986 *Progress of theoretical physics* **75** 442–444
- [39] Zhou Y, Cao C and Zhang F C 2017 *Science Bulletin* **62** 208
- [40] Wu X, Yang F, Le C, Fan H and Hu J 2015 *Physical Review B* **92** 104511
- [41] Xu C, Wu N, Zhi G X, Lei B H, Duan X, Ning F, Cao C and Chen Q 2020 *NPJ Computational Materials* **6** 1–8
- [42] Watson M, Feng Y, Nicholson C, Monney C, Riley J, Iwasawa H, Refson K, Sacksteder V, Adroja D, Zhao J et al. 2017 *Physical review letters* **118** 097002
- [43] Ōnuki Y, Settai R, Haga Y, Machida Y, Izawa K, Honda F and Aoki D 2014 *Comptes Rendus Physique* **15** 616–629
- [44] Nomoto T and Ikeda H 2016 *Physical review letters* **117** 217002
- [45] Sauls J 1994 *Advances in Physics* **43** 113–141
- [46] Scalapino D, Loh Jr E and Hirsch J 1986 *Physical Review B* **34** 8190

- [47] Scalapino D, Loh Jr E and Hirsch J 1987 *Physical Review B* **35** 6694
- [48] Schrieffer J 1964 *Theory of superconductivity* (NewYork)
- [49] Schrieffer J, Wen X and Zhang S 1989 *Physical Review B* **39** 11663
- [50] Monthoux P, Balatsky A and Pines D 1991 *Physical review letters* **67** 3448
- [51] Scalapino D J 2012 *Reviews of Modern Physics* **84** 1383
- [52] Davis J S and Lee D H 2013 *Proceedings of the National Academy of Sciences* **110** 17623–17630
- [53] Das T, Markiewicz R and Bansil A 2014 *Advances in Physics* **63** 151–266
- [54] Adhikary P and Das T 2020 *Physical Review B* **101** 214517
- [55] Adhikary P and Das T 2020 *Physical Review B* **101** 214517
- [56] Mazin I, Singh D J, Johannes s M and Du M H 2008 *Physical Review Letters* **101** 057003
- [57] Graser S, Maier T, Hirschfeld P and Scalapino D 2009 *New Journal of Physics* **11** 025016
- [58] Yao Z J, Li J X and Wang Z 2009 *New Journal of Physics* **11** 025009
- [59] Das T and Balatsky A 2011 *Physical Review B* **84** 014521
- [60] Chubukov A 2012 *Annu. Rev. Condens. Matter Phys.* **3** 57–92
- [61] Takimoto T, Hotta T and Ueda K 2004 *Physical Review B* **69** 104504
- [62] Das T, Zhu J X and Graf M J 2015 *Scientific reports* **5** 1–8
- [63] Das T, Zhu J X and Graf M J 2015 *Scientific reports* **5** 1–8
- [64] Ikeda H, Suzuki M T and Arita R 2015 *Physical review letters* **114** 147003
- [65] Adhikary P and Das T 2019
- [66] Chubukov A, Pines D and Schmalian J 2003 A spin fluctuation model for d-wave superconductivity
The Physics of Superconductors (Springer) pp 495–590
- [67] Scalapino D J 2012 *Reviews of Modern Physics* **84** 1383
- [68] Das T, Markiewicz R and Bansil A 2014 *Advances in Physics* **63** 151–266
- [69] Kubo K 2007 *Physical Review B* **75** 224509
- [70] Das T and Balatsky A 2012 *Journal of Physics: Condensed Matter* **24** 182201
- [71] Das T, Vorontsov A B, Vekhter I and Graf M J 2012 *Physical review letters* **109** 187006
- [72] Bhattacharyya A, Panda K, Adroja D, Kase N, Biswas P, Saha S, Das T, Lees M and Hillier A
2019 *Journal of Physics: Condensed Matter* **32** 085601